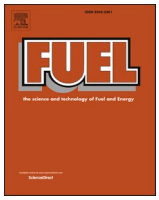
Fuel 381 (2025) 133233



Contents lists available at ScienceDirect

Fuel

journal homepage: www.elsevier.com/locate/fuel



Full Length Article



# Transient plasma enhanced combustion of ultra-lean $H_2$ in an internal combustion engine for reduced $NO_x$ emission

Boxin Zhang [d,1], Mariano Rubio [e,1], Joshua E. Tobar Lam [h], Aimee Ortiz-Ramirez [g], Travis Riggs [h], Oscar Hernandez [f], Yushan Chen [g], Caleb Medchill [c], Fokion Egolfopoulos [e], Stephen B. Cronin [a,b,c,*]

[a] Department of Physics and Astronomy, University of Southern California, Los Angeles, CA 90089, USA
[b] Department of Chemistry, University of Southern California, Los Angeles, CA 90089, USA
[c] Ming Hsieh Department of Electrical Engineering, University of Southern California, Los Angeles, CA 90089, USA
[d] Mork Family Department of Chemical Engineering and Materials Science, University of Southern California, Los Angeles, CA 90089, USA
[e] Department of Aerospace and Mechanical Engineering, University of Southern California, Los Angeles, CA 90089, USA
[f] Department of Civil Engineering, Citrus College, Glendora, CA 91741, USA
[g] Department of Mechanical Engineering, Citrus College, Glendora, CA 91741, USA
[h] Automotive Technology, Citrus College, Glendora, CA 91741, USA

ARTICLE INFO

*Keywords:*
Transient plasma ignition
Internal combustion
Carbon-free fuel
Greenhouse gas
Hydrogen combustion

ABSTRACT

Hydrogen is considered one of the leading candidates among all carbon-free (i.e., "green") fuels. While the combustion of hydrogen does not produce any $CO_2$ emissions, it results in high $NO_x$ emissions (i.e., NO and $NO_2$) due to its high flame temperatures. Here, we report substantial improvements in the combustion of $H_2$ under ultra-lean conditions using transient plasma ignition (TPI), which supports stable engine operation with minimal $NO_x$ emissions. The transient plasma-based ignition system was tested on a retrofitted natural gas engine using zero-carbon fuel (i.e., $H_2$). The flame characterization was conducted in a canonical static combustion chamber together with a high-speed camera and a pressure sensor. Compared to conventional spark ignition (magneto type), the TPI enables a 2-fold improvement in engine stability (i.e., 52 % drop in coefficient of variation of indicated mean effective pressure ($COV_{IMEP}$) at an engine speed of 1500 RPM) and a 4-fold reduction in $NO_x$ emissions at constant power at an engine speed of 2400 RPM. In this ultra-lean range, we also observe a 175 % increase in the maximum mechanical power produced by the engine using TPI (0.2 kW at an engine speed of 1100 RPM) by achieving more complete combustion. We compare the results of engine performance (stability, power, and $NO_x$ emissions) with those using a conventional (magneto-type) spark ignition (CSI) over a wide range of equivalence ratios ($\phi$) from 0.2 to 0.7. The transient plasma-based enhancement arises from hydrodynamic effects, (i.e., ionic winds), which gives rise to turbulence and multi-scale mixing. This is supported by Schlieren imaging, which shows an augmented flame surface area and reduced ignition delays with TPI compared to that with CSI. This general approach enables hydrogen fuel to be burned in internal combustion engines, while maintaining low $NO_x$ emissions using a transient plasma ignition system that could serve as a drop-in replacement of conventional magneto-type ignition systems without requiring any further engine modifications.

## 1. Introduction

While rechargeable Li-ion batteries are capable of powering small passenger vehicles, they do not provide sufficient energy storage for large vehicles, such as long-haul trucking and locomotives, as reported by Giuliano et al. [1,2] As such, technologies addressing this wide scale need for clean combustion in larger engines are much needed particularly within the transportation sector, thus, meeting the demand for advanced vehicle technologies and sustainable freight. In the general public, there is a common misconception that electric vehicles will

* Corresponding author at: Department of Electrical Engineering, University of Southern California, 3737 Watt Way, PHE 624, Los Angeles, CA, 90089, USA.
*E-mail address:* scronin@usc.edu (S.B. Cronin).
[1] Boxin Zhang and Mariano Rubio contributed equally to this work.

https://doi.org/10.1016/j.fuel.2024.133233
Received 23 February 2024; Received in revised form 30 August 2024; Accepted 18 September 2024
Available online 25 September 2024
0016-2361/© 2024 Elsevier Ltd. All rights are reserved, including those for text and data mining, AI training, and similar technologies.

eliminate all environmental concerns associated with transportation. However, "zero emissions" simply means zero "tailpipe" emissions, and the electricity used to power these vehicles is predominantly produced by burning fossil fuels. As such, electric vehicles can have relatively high $CO_2$ equivalent emissions, and more advanced systems, approaches, and technologies for enabling clean combustion need to be explored.

Hydrogen ($H_2$) is considered to be an excellent green-fuel candidate for spark ignition engines due to its ability to burn under ultra-lean conditions, as well as its high flame speeds and low ignition energies [3]. Research on $H_2$ combustion in engines has been conducted by a variety of industries and research groups. In 2007, BMW built a 6-liter V-12 motor hydrogen combustion vehicle based on the BMW 7 Series (760Li) [4]. Ford developed the P2000 hydrogen engine to power Ford's E-450 Shuttle Bus [3]. Along with a fuel transfer system, liquid $H_2$ was used in internal combustion engines for improved performance with zero exhaust emissions [5]. Under optimal operating conditions, similar efficiencies compared to diesel engines can be achieved with high-pressure direct injection (HPDI) operation [6].

While $H_2$ is a carbon-free fuel and does not produce any $CO_2$ emissions, its utilization in engines is limited by knock, preignition, and low power densities. It is well established that the flammable and adiabatic flame temperature ($T_{ad}$) ranges of $H_2$ are much wider than those of hydrocarbons. One of the main challenges associated with hydrogen combustion is low engine stability. The $COV_{IMEP}$ ratio increases by more than twice when hydrogen is added to a conventional engine [7]. Luo *et al.* observed comparatively low engine stability (i.e., high $COV_{IMEP}$) at lower hydrogen equivalence ratios [8]. Another challenge is high $NO_x$ emissions. For near-stoichiometric conditions, $T_{ad} \sim$ 2,300–2,400 K results in high thermal $NO_x$ production [9–12]. The maximum NO emission measured with hydrogen can be almost twice that of traditional hydrocarbon fuels, e.g., isooctane [13]. The $NO_x$ emission increases rapidly when the equivalence ratio of hydrogen is larger than 0.5 [14]. Jamrozik's group observed an over 80 % increase in $NO_x$ emissions (from 476 ppm to 860 ppm) by adding hydrogen to a diesel engine [7]. However, under lean conditions (i.e., equivalence ratios $\phi < 1$), $T_{ad}$ can be lower than the $NO_x$ formation threshold (~1700 K) while the laminar flame speed ($S_u^o$) is high enough to assure robust burning rates. Additionally, at $\phi < 1$ $H_2$/air flames develop thermo-diffusional instabilities that could compromise the overall combustion stability in internal combustion engines. It should be noted that $H_2$ has high auto-ignition temperatures (i.e., high octane number), but low ignition energy (i.e., increased preignition propensity) resulting in low preignition-limited $\phi$ and thus reduced energy density. While using the octane number to compare hydrogen's anti-knocking characteristics might seem sufficient for describing its ability to withstand compression before ignition, the methane number offers a more accurate comparison of a gaseous fuel's resistance to knocking. On a scale of 0–100, with pure methane at 100 (the most resistant to knocking) and pure hydrogen at 0 (the least resistant), it is important to emphasize that the engine operating characteristics must match those required to run pure hydrogen fuel and equivalence ratios close to 1. Additionally, pre-ignition poses a constraint on an engine's operation capability to run on pure hydrogen fuel at equivalence ratios close to 1. This is related to the minimum ignition energy required to ignite hydrogen [15]. As a result, the practical engine investigations were conducted within the leaner fuel mixture range to avoid making major engine modifications that would significantly alter the engine's characteristics from those

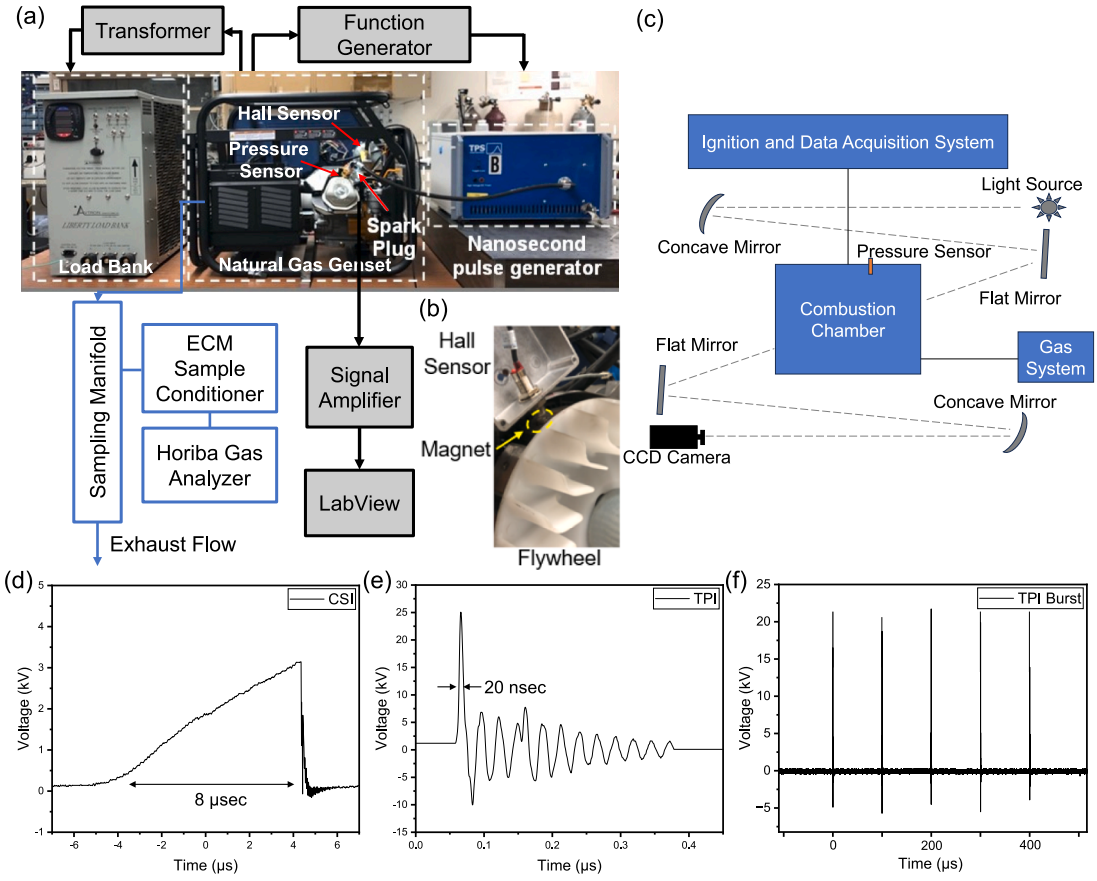



**Fig. 1.** (a) Photograph and schematic diagram of the multi-gas engine test platform with modified nanosecond pulse transient plasma ignition (TPI) system and exhaust gas characterization configuration. (b) Photograph of the customized TPI trigger system. (c) Schematic diagram of the constant volume combustion chamber system. Voltage waveform plots for (d) conventional spark ignition (CSI) and (e) transient plasma ignition (TPI). (f) Waveform plot for a plasma burst of 5 pulses discharged at 10 kHz.

currently used for gasoline or methane. The limitations of $H_2$-powered engines can potentially be addressed by ignition control, port-fuel-injection vs. direct injection, and fuel stratification, which are based on thermo-chemical principles. It was reported that ultra-lean combustion produces a low-temperature flame, which leads to lower $NO_x$ emissions and reduced heat transfer to the walls, resulting in higher engine efficiency [10]. Lean burns require higher starting pressures to achieve a low enough equivalence ratio to avoid unstable combustion and high $NO_x$ emissions while maintaining sufficient torque and power [16]. A potential method to achieve this is through advanced ignition systems. Work done by Singleton *et al.* revealed that a transient plasma discharge in a hydrocarbon fuel–air mixture created ignition sites at multiple spatially separated locations, particularly where the greatest production of active species occurred due to electron impact excitation, dissociation, and ionization [17]. Cathy *et al.* reported that transient plasma enabled stable lean combustion of hydrocarbon fuels at levels that were not otherwise realizable by spark ignition, and the 20-ns pulse was able to increase peak pressure by 20 % compared to conventional spark ignition [18]. Our work aims to explore the possibility of augmenting the engine's stable operational limits via a non-thermal Transient Plasma (TP) and introduce an additional external control degree of freedom to complement the established aforementioned approaches.

This TP approach has been used previously to reduce $CO_2$ emissions and improve the combustion of natural gas (NG), the main constituent of which is $CH_4$. In previous research works, many alternative ignition methods have been used on hydrogen combustion engine. A coil-on-plug system was used to avoid induction ignition in an adjacent cable [19]. A higher voltage output ignition system was applied to provide enough secondary ignition voltage for the combustion of hydrogen mixtures [20–22]. Different spark plug gaps were tested for better engine performance of hydrogen combustion [23]. Recent studies using nanosecond pulsed discharge [24], high-frequency streamer discharge [25], and filamentary discharge [26] have shown that plasma can improve fuel/air mixing, ignition, and flame stability by enhancement mechanisms involving thermal, chemical, and plasma-induced aerodynamic effects. For internal combustion engines, effective demonstrations of plasma-assisted ignition and combustion have been achieved using single and multi-spark discharges [27], nanosecond pulsed discharge [28], and radio frequency discharge [29]. In addition, plasma has also been used to control emissions, in which case effectively reduced $NO_x$ emission was achieved by using a pulsed discharge [30]. The role of hydrodynamic forces on the ignition of lean $CH_4$-air mixtures has been discussed by Pineda et al. [31] High-speed Schlieren imaging revealed the significant role of hydrodynamics in the observed enhancement, including a more wrinkled flame kernel structure and increased burning rates from the increased flame surface area. Increasing the number of nanosecond pulses per ignition event (i.e., burst number) increases the expulsion of the flame kernel. In TPI, multiple pulses of transient plasma are discharged across the spark gap, resulting in properties that are very different from that of CSI. Here, TPI provides higher voltages (~20 kV) over an extremely short time scale (~20 ns), which can easily cause breakdown of molecular bonds, resulting in the formation of radicals, e.g., atomic H and atomic O, as illustrated in Figure S1 in the Supplemental Document. These radicals or ions are accelerated by forces produced by the electric field, causing movement of the ions that eventually form ionic winds [32]. The hypothesis is that using multiple pulses in an already ionized medium allows for the creation of ionic winds and, thus, for a more effective ignition and enhancement of the combustion process through mixing and a transition to turbulence in its early stages and beyond. However, this phenomenon has yet to be observed in or applied to carbon-free fuels.

## 2. Experimental Details

The TP-based ignition system was tested on a retrofitted NG engine using zero-carbon fuel (i.e., $H_2$) and compared to results obtained from the same engine with a conventional spark (i.e., magneto-type) ignition system. The tests performed involved measuring and quantifying the exhaust gas composition of $CO_2$ and $NO_x$, maximum power output, as well as the cylinder pressure. Fig. 1 depicts the experimental setup, which uses a 5.5 kW multi-fuel generator consisting of a 439 cc, 4-stroke engine with a 9.56:1 compression ratio (Firman T08071). The 1 in. bore engine carburetor was left intact, and gaseous fuel was fed through the natural gas inlet port. The original ignition system, consisting of a permanent magnet attached to the flywheel with a magneto ignition coil rated at 80 mJ with integrated spark plug wire, was left in place and disabled during TPI testing using a coil grounding circuit. A manifold absolute pressure sensor was installed in the intake manifold to measure inlet pressure, and volumetric flow rate meters were used to measure control engine air and fuel entering the engine. In the comparison between conventional spark ignition (CSI) and transient plasma ignition (TPI), the magneto-type ignition system on the engine has been replaced by a nanosecond high-voltage pulse generator (Transient Plasma System Inc., Model 20X) using an electromagnetic pickup (i.e., Hall-effect sensor, as shown in Figure S2 in the Supplemental Document) that provides a trigger signal for the nanosecond pulse generator. This high voltage nanosecond pulse generator is capable of producing peak pulse voltages up to 20 kV at pulse repetition rates up to 10 kHz. Each pulse has a duration (i.e., pulse lifetime) of ~ 20 ns and a peak voltage of ~ 25 kV, as plotted in Fig. 1e. The system can also be programmed to produce a short burst of pulses. For each combustion event, our TPI system produces a burst of 5 pulses separated 100 μs (i.e., 10 kHz), as shown in Fig. 1f. To first order, the peak voltages (within each burst) remain consistent even after the initiation of the flame kernel. While these peak voltages do not change, the reflected power can change with load impendence and the associated impedance mismatch. In the Schlieren imaging videos (in the Supporting Information), we see bright flashes corresponding to the 5 separate plasma discharges. Figure S2a shows the conventional ignition coil system, and Figure S2b shows the customized TPI system where a Hall sensor has been installed above the flywheel to pick up a trigger signal from a magnet mounted on the flywheel each time they align during the combustion cycle. A standard J-gap spark plug with a gap distance of 0.965 mm is used for CSI, whereas for TPI the flat tip of the spark plug has been removed for better ignition leaving a much larger gap of ~ 4 mm (see Figure S3 in the Supplemental Document). The increased spark gap distance plays an important role in the TPI process by enabling longer streamers to be produced, increasing ionization and hydrodynamic effects. The CSI could not generate a spark discharge with gaps larger than 0.965 mm. One of TPI's primary advantages is its ability to discharge plasma across gaps that are four times larger than those achievable with CSI. This is particularly important for promoting hydrodynamic effects (i.e., ionic winds). Since the flame is a weakly ionized gas, the 2nd – 5th pulses experience rapid acceleration from the applied high voltage pulses, which gives rise to turbulence and multi-scale mixing. The tests conducted here used a non-resistor-type spark plug to minimize the engine modifications. The only alteration was to enlarge the electrode gap by trimming the outer electrode (see Figure S3). This takes advantage of the transient pulsed plasma's ability to create streamers across larger gaps and induce turbulence by inducing ionic movement. Also, we used a high voltage coaxial cable (instead of a standard spark plug cable) to minimize electromagnetic interference (EMI). Figures S3a and S3b in the Supplemental Document show photographs of the standard J-gap and customized spark plugs. The engine exhaust then flows through our sampling manifold, which consists of a sample conditioner (ECM) and Horiba portable gas analyzer (PGA) enabling us to measure and quantify $CO_2$, $NO_x$, and $O_2$, as illustrated in Fig. 1a. In addition, a pressure sensor has been installed in the engine cylinder that allows for the determination of the coefficient of variation of indicated mean effective pressure ($COV_{IMEP}$), a key metric of engine stability. A load bank (Avtron LPH75) is connected to the engine genset, and the power output is controlled by a variable transformer. To determine the equivalence ratio of the engine, a gas analyzer with an

oxygen sensor was used, and the percentage of oxygen in the exhaust stream was measured. The measured percentage of oxygen was then used to calculate the exhaust-based equivalence ratio using the following:

$$\Phi = \frac{1 - \frac{4.76(\%O_2)}{100}}{1 + \frac{\%O_2}{100}} \quad (1)$$

where no oxygen remaining in the exhaust would represent an equivalence ratio of $\Phi = 1$ [33].

Fig. 1b shows our customized TPI trigger system where a magnet has been installed on the flywheel, which triggers the Hall-effect sensor when aligned with each other as the crankshaft spins. The Hall-effect signal served as both the TPI trigger signal and the RPM signal used for engine cycle calculations. The ignition timing for TPI can be adjusted by changing the magnet position. To directly compare the effects of flame propagation without the influence of ignition timing, the ignition timing was held at a constant 10 degrees before top dead center (BTDC) for both the CSI and TPI systems. The RPM was purposely prevented from going beyond 4000 RPM to focus on the engine's power output and COV without the added advantage of a spark timing curve. When triggered by a digital signal from the Hall sensor, a function generator (Stanford Research Systems Model DG 645) outputs a burst of 5 digital signals at 10 kHz that are sent to the nanosecond pulse generator for each combustion stroke. The nanosecond pulse generator then produces a burst of 5 TP discharges at the tip of the customized spark plug. The Schlieren imaging system consisted of a Phantom V710 camera with focused LED light source, and an NI USB-6259 DAQ used in conjunction with LabVIEW to output the recording trigger signal and the pulse generator trigger signal and to collect dynamic pressure sensor data from a Kistler charge amplifier (603CAA) during combustion, as shown in Fig. 1c. The chamber was custom-designed with quartz glass windows, and curved mirrors were utilized to focus the reflected light image. The chamber was filled using needle valves, and the filling pressure was monitored via 5 psi, 15 psi, and 50 psi Omega PX309 pressure sensors. The initial pressure of the unburned mixture in the combustion chamber is 1 atmosphere. The partial pressure of the reactants was calculated by molar their fractions, and the gases were introduced one reactant at a time, starting with the lowest partial pressure reactant. To allow gas mixing and gas settling in the chamber, a 5-minute waiting period was given before the gas mixture was ignited. During experimentation, frame recording was set to 13,000 fps. The discharge electrode gap was set to 1.5 mm.

Waveform plots of CSI and TPI are plotted in Fig. 1d and 1e. Here, the nanosecond pulse is 2–3 orders of magnitude faster than that of the conventional spark and reaches much higher peak voltages/electric fields. It has been firmly established in published studies that multiple nanosecond pulse discharges improve the combustion characteristics of hydrocarbon fuels [31,34–45]. However, the improvement in the combustion characteristics of this carbon-free fuel (i.e., $H_2$) with multiple pulse discharges has yet to be fully understood. Our hypothesis is that, since the kernel/flame behaves as a weakly ionized plasma, it is likely that the 2nd − 5th pulses affect the shape of the kernel/flame by the strong applied electric fields. Previous studies using multiple pulse discharges have demonstrated hydrodynamic effects in mixtures of NG with air [31]. In the work presented here, in each combustion event, our TPI system produces a burst of 5 pulses at a frequency of 10 kHz, as illustrated in Fig. 1f. Each pulse has a duration (i.e., pulse lifetime) of ~ 20 ns and a peak voltage of ~ 25 kV, as illustrated in Fig. 1e. We found that engine performance improved with an increased number of pulses (per burst) and higher frequencies (within each burst), as long as the total discharge time did not exceed the initial 2 ms of the combustion event. After testing various combinations of pulse numbers and frequencies, we found that 5 pulses at 10 kHz yielded the best results, representing the optimal condition we could achieve. This was accomplished with an electrical energy expenditure of less than 20 mJ per pulse, which is less than 0.01 % of the power produced by the engine. The corresponding voltage waveforms of both ignition types are shown in Fig. 1d, 1e, and 1f. The CSI consumes 56 mJ per ignition event, which is roughly half that of the TPI, which consumes 100 mJ, so it is unlikely that the enhancement we were seeing is simply due to high ignition energies. The instantaneous power, on the other hand is quite different for these two ignition systems. The CSI delivers 56 mJ in 8 μsec (instantaneous power = 7 kW), whereas the TPI discharges 20 mJ/20nsec (instantaneous power = 1 MW), which corresponds to an enhancement of 142X in instantaneous power.

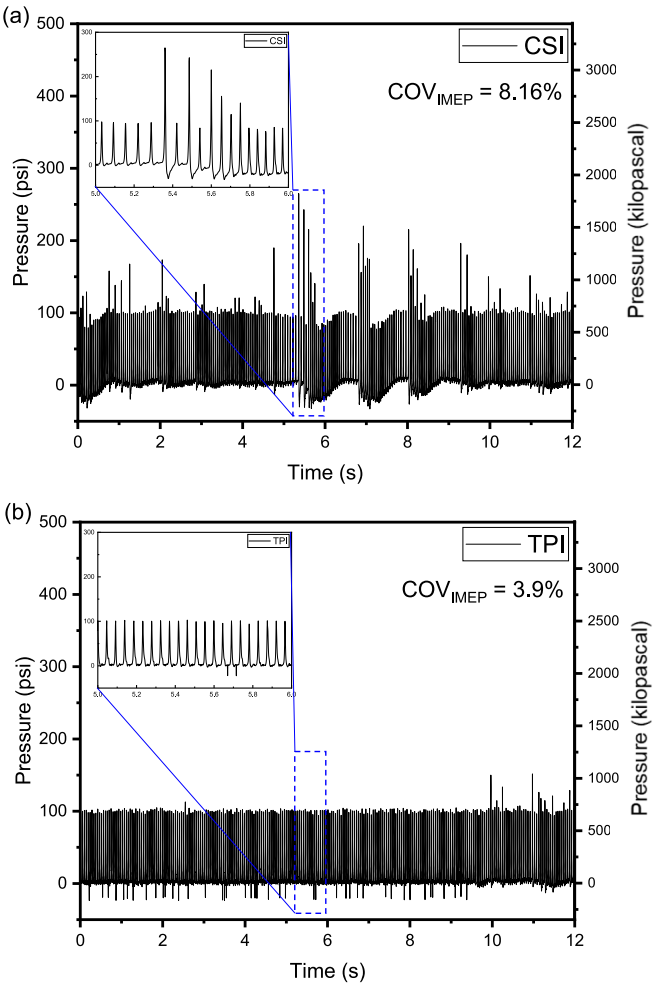



**Fig. 2.** Chamber pressure plots for (a) conventional spark ignition (CSI) and (b) transient plasma ignition (TPI) at $\phi \sim 0.3$ under no-load conditions.

The engine was disassembled to obtain the measurements of the bore (B), stroke (L), crank radius (a), and connecting rod length (l), which were then used to calculate the corresponding volume change (ΔV) with respect to different crank angles (θ). Table S1 in the Supplemental Document provides the engine mechanical specifications. The crank angle measurement used in the COV calculation utilized a 2500 pulse per rotation encoder mounted to the rear of the generator rotor spinning with the crankshaft. This setup provided a resolution of 0.114°, with the TDC crankshaft position determined by the output signal of the Hall-effect sensor, which also triggered the function generator for the TPI pulser. The clearance volume ($V_c$) was also measured and, along with the calculated swept volume ($V_s$), the compression ratio was determined. Equations (2) and (3) were used to calculate the cylinder volume at each crank angle measured [46].

$$V_j = V_c + \frac{\pi B^2}{4} C \quad (2)$$

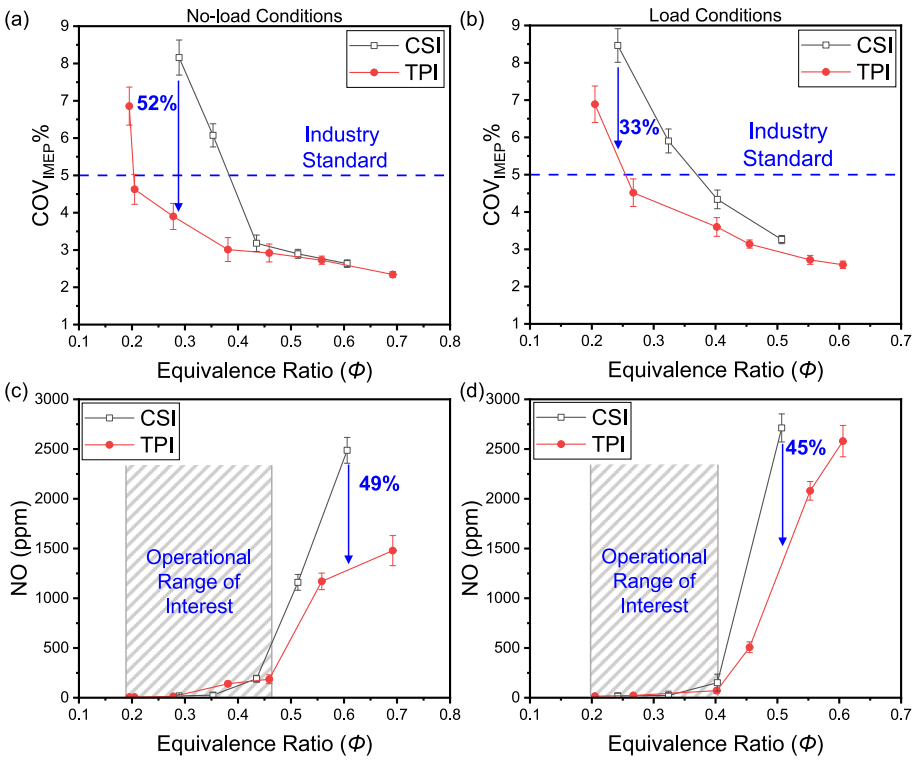



**Fig. 3.** Coefficient of variation of the indicated mean effective pressure ($COV_{IMEP}$) plotted as a function of equivalence ratio ($\phi$) plots for (a) no-load conditions and (b) constant load conditions. Corresponding NO emissions plotted as a function of $\phi$ for (c) no-load and (d) load conditions.

$$C = \frac{L}{2}\{R + 1 - \cos\theta - [R^2 - (\sin\theta)^2]^{\frac{1}{2}}\} \quad (3)$$

where $V_j$ is the cylinder volume at a particular crank angle, $\theta$ is the crank angle, and $R$ is the ratio of the rod length to the crank radius, $R = l/a$. The output signals from both the pressure transducer and the Hall-effect sensor were collected using LabView software to determine the cylinder pressure and RPM, respectively. The indicated mean effective pressure (IMEP) was determined by using cylinder pressure measurements along with the calculated volume changes and discretizing the piston work performed relative to the number of samples obtained for each cycle by using Equation (4) [47].

$$IMEP = \frac{1}{V_s}\sum_{j=0}^{n-1}\frac{(P_{j+1} + P_j)}{2}(V_{j+1} - V_j) \quad (4)$$

where $V_s$ is the displacement (swept) volume, $P_{j+1}, P_j$ is the $j+1$st and $j^{th}$ combustion chamber pressures, $V_{j+1}, V_j$ is the $j+1st$ and $j^{th}$ combustion chamber volumes and $n$ is the number of sampling data taken per cycle. The coefficient of variance of the indicated mean effective pressure ($COV_{IMEP}$) is calculated using the following equation:

$$COV_{IMEP}\% = \frac{\sigma}{IMEP_{mean}}(100) = \frac{\sqrt{\frac{\sum (IMEP_i - IMEP_{mean})^2}{N}}}{IMEP_{mean}}(100) \quad (5)$$

where $\sigma$ is the standard deviation, $IMEP_{mean}$ is the mean of the IMEPs of all cycles recorded, $IMEP_i$ is the IMEP of each cycle, and $N$ is the total number of cycles.

## 3. Results and Discussion

Fig. 2 shows the chamber pressure plots comparing CSI and TPI over 100 combustion cycles for no-load conditions. Here, we observe significantly more variability in the peak cylinder pressure with CSI than with TPI. This data shows that the engine was able to run more stably with TPI than with CSI, and the $COV_{IMEP}$ provides a quantitative metric of this improvement in combustion/engine stability. 5 % $COV_{IMEP}$ is considered to be the highest percentage tolerable for production engines [25] and, with TPI, we were able to substantially extend the stable $H_2$ combustion range to ultra-lean conditions, where $NO_x$ emissions are minimal. The engine speeds are 1520 RPM for TPI and 1480 RPM for CSI, representing comparable engine conditions.

**Table 1**
Tables for engine RPM and power output at different $\phi$ under no-load and load conditions.

| No-load Condition | | | Load Condition | | | |
|---|---|---|---|---|---|---|
| | $\phi$ | RPM±50 | | $\phi$ | RPM±50 | power |
| CSI | 0.606 | 2352 | CSI | 0.507 | 1915 | 0.68 |
| | 0.513 | 2236 | | 0.403 | 2158 | 0.44 |
| | 0.435 | 2038 | | 0.324 | 2020 | 0.29 |
| | 0.353 | 1773 | | 0.242 | 1913 | 0.08 |
| | 0.289 | 1480 | TPI | 0.606 | 1825 | 0.84 |
| TPI | 0.692 | 2450 | | 0.553 | 1801 | 0.77 |
| | 0.558 | 2287 | | 0.455 | 1631 | 0.68 |
| | 0.459 | 2044 | | 0.402 | 1486 | 0.52 |
| | 0.381 | 1860 | | 0.267 | 1123 | 0.31 |
| | 0.278 | 1520 | | 0.205 | 1035 | 0.12 |
| | 0.205 | 1011 | | | | |
| | 0.195 | 802 | | | | |

Fig. 3 shows the results for $COV_{IMEP}$ vs. $\phi$ with both CSI and TPI under no load and constant load conditions (Fig. 3a and 3b), along with the corresponding NO emissions (Fig. 3c and 3d). Under ultra-lean conditions (i.e., $0.2 \leq \phi \leq 0.4$), we were able to decrease the $COV_{IMEP}$ by as much as 52 % and 33 % under no load and load conditions, respectively, as illustrated in Fig. 3a and 3b. In Fig. 3c and 3d, a nearly 50 % reduction in NO emission was achieved with TPI for $0.5 \leq \phi \leq 0.6$ under both no load and load conditions. Minimal NO was observed under $\phi < 0.4$ due to the low $T_{ad}$ values. Under both no load and load conditions, TPI enables stable engine operation ($COV_{IMEP}$<5%) with

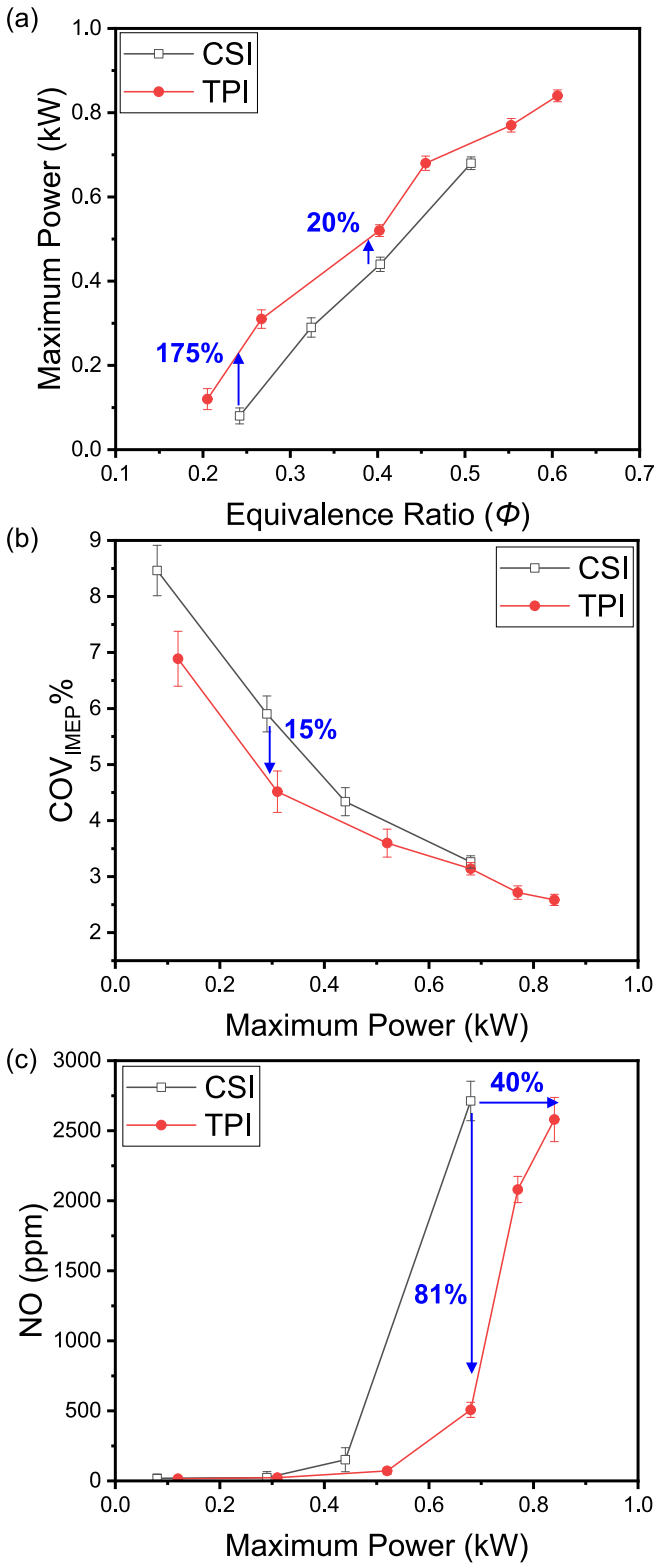



**Fig. 4.** Plots comparing CSI and TPI for (a) maximum power vs. $\phi$, (b) $COV_{IMEP}$ vs. maximum power, and (c) NO emissions vs. maximum power.

ultra-lean $H_2$ (i.e., $0.2 \leq \phi \leq 0.4$) in order to mitigate $NO_x$ emission, which is not otherwise achievable with CSI. The ignition timing was held at 10 degrees BTDC for both CSI and TPI under all experimental conditions. Under no-load conditions, the engine speed increased as the fuel mixture became richer for both CSI and TPI. When applying loads, the engine speed increased proportionally with the equivalence ratio for

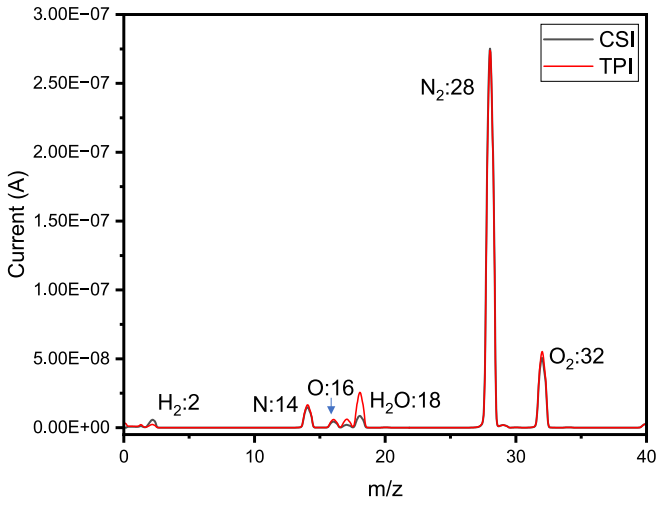



**Fig. 5.** Plot of mass spectrometry (MS) measurement results of the exhaust gas with both CSI and TPI at $\Phi = 0.25$, showing more complete combustion with TPI.

TPI, whereas the engine speed stayed near 2000 RPM with CSI over the whole equivalence ratio range. The corresponding data is presented in Table 1.

Fig. 4 shows the maximum power output (Fig. 4a), $COV_{IMEP}$ with respect to various loads (Fig. 4b), and the corresponding NO emissions (Fig. 4c) under various load conditions with CSI and TPI. Here, we define the maximum power as when the power stopped increasing and the RPM started to decrease at the same time. Fig. 4a shows a minimum of 20 % increase in maximum power output with TPI measured when $\phi = 0.3 \sim 0.5$. More importantly, under ultra-lean conditions $\phi = 0.24 \sim 0.3$, the maximum power output was elevated by up to 175 % with TPI indicating more complete combustion. Fig. 5 shows mass spectrometer (MS) measurements of the exhaust gas produced with both CSI and TPI at $\phi = 0.25$. We observed a lower $H_2$ ($m/z = 2$) signal with TPI than CSI, demonstrating more complete combustion with TPI. In addition, more $H_2O$ ($m/z = 18$) was detected with TPI as the main product of burning $H_2$, confirming more complete $H_2$ combustion. It is difficult to achieve complete $H_2$ combustion under ultra-lean conditions. Here, TPI gives rise to more complete combustion compared to CSI due to the enhanced hydrodynamic effects and flame stability. In addition, the $H_2$ combustion range was significantly extended from $\phi = 0.5$ to $\phi = 0.6$ with TPI. Under maximum load conditions (i.e., maximum power), up to 15 % reduction in $COV_{IMEP}$ was observed with TPI (Fig. 4b), which means that the engine was able to run more stably while outputting the same amount of power as with CSI. We also observe an 81 % reduction in NO emissions with TPI when measured under 0.7 kW load, as plotted in Fig. 4c. While the peak NO emissions obtained with TPI are shifted to higher $\phi$, 40 % more power output was achieved with TPI than with CSI.

One of the key challenges in burning $H_2$ in an internal combustion engine is the thermo-diffusional flame instabilities that develop under lean fuel conditions. The TPI enables more stable combustion by initiating a more robust ignition kernel. This arises due to the generation of highly reactive radical species such as atomic O, atomic H, and ozone ($O_3$), as well as hydrodynamic effects which introduce turbulence and multiscale mixing in the early stage of the combustion process. This improved combustion enables robust and stable combustion at ultra-lean conditions under which the flame temperatures are substantially lowered below the threshold for $N_2$ oxidation via the Zeldovich mechanism [48]. While the plasma itself produces a small amount of NO due to atomic oxygen radicals [49], this is negligible compared to that produced by the $H_2$ combustion processes via the Zeldovich mechanism (i.e., high flame temperatures) [48]. This can be seen in Fig. 3c and 3d. Over the range from $\phi = 0.2 - 0.6$, the direct plasma-generated NO is

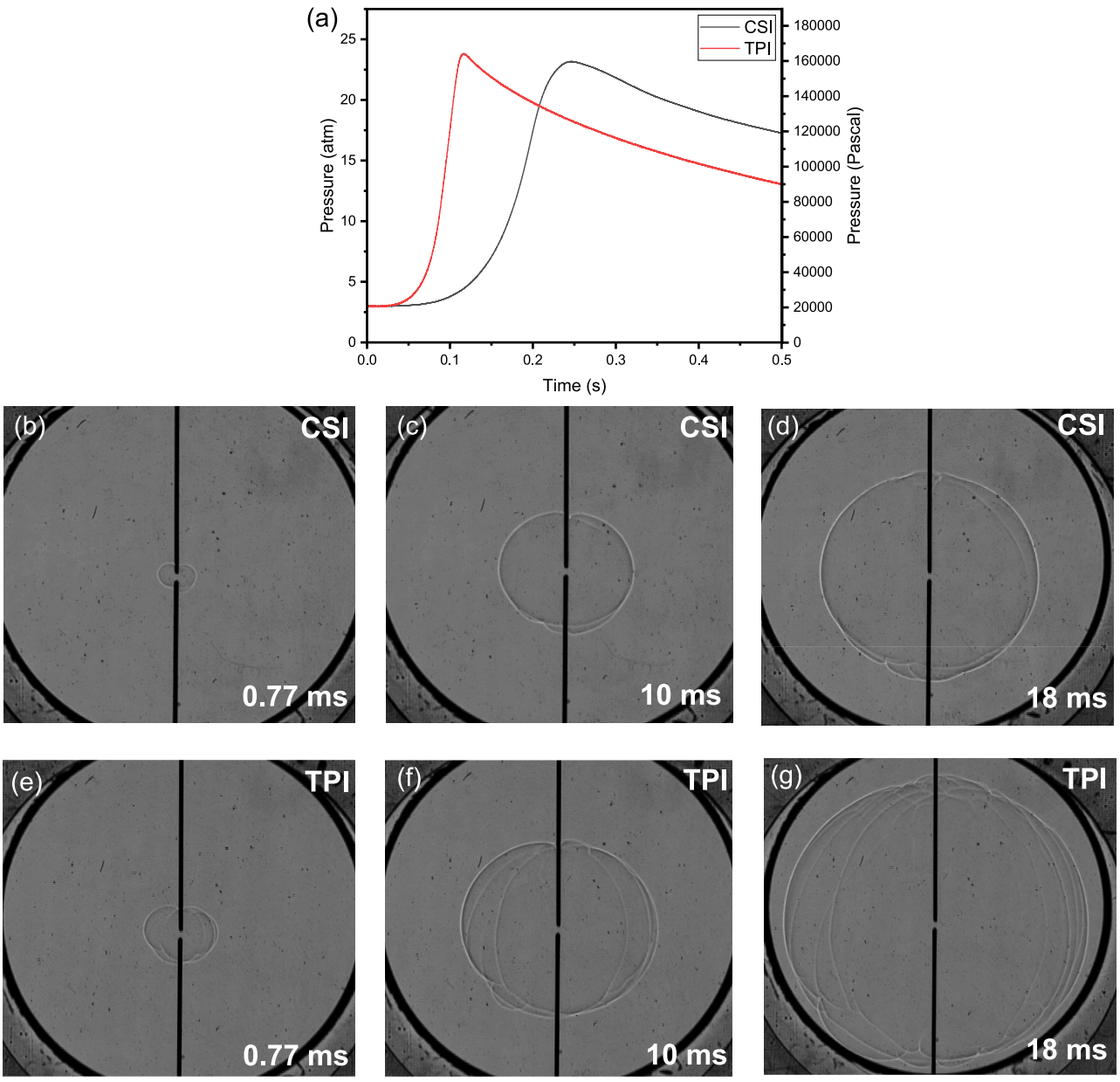



**Fig. 6.** (a) Chamber pressure curves of the combustion events with $\phi = 0.4$ using both CSI and TPI. Screenshots of the high-speed videos of the combustion events at different times with (b-d) CSI and (e-g) TPI.

constant. The massive increase in NO observed above $\phi > 0.4$ corresponds to NO generated by the high flame temperature-driven breakdown of $N_2$ in air.

To obtain a more fundamental understanding of the transient plasma-based enhancement mechanism, we performed high-speed imaging of the flames in a constant volume combustion chamber with $\phi = 0.4$ using both CSI and TPI, as shown in Fig. 6. The corresponding chamber pressure vs. time curves demonstrate substantially reduced ignition delays and faster pressure rise times (i.e., dP/dt) with TPI compared to that obtained with CSI (Fig. 6a). This data shows quantitative enhancement in the flame speed and reduction in the delay of flame propagation as shown by the difference in pressure rise delay under these ultra-lean conditions. The Schlieren imaging provides clear evidence of ionic winds and hydrodynamic effects, which give rise to turbulence and mixing, as demonstrated by the wrinkled flame structure, resulting in elevated instabilities that ultimately contribute to increased flame surface area and flame stability. The full videos are available in the online Supporting Information. In addition, the pressure and crank position were recorded to determine the COV and to compare the heat release rate during the flame propagation period with respect to the crank angle (dQ/dθ). The ignition timing was held at 10 degrees BTDC for both CSI and TPI to allow for a direct comparison of the heat release rate. The heat release rate was calculated using

$$\left(\frac{dQ}{d\theta}\right) = \frac{\left(\frac{VdP}{d\theta}\right) + \gamma P\left(\frac{dV}{d\theta}\right)}{\gamma - 1} - \frac{PV}{(\gamma - 1)^2}\left(\frac{d\gamma}{d\theta}\right) \quad (6)$$

where dQ/dθ is the heat release, V is the cylinder volume, P is the cylinder pressure, θ is the crank position, and γ the specific heat ratio [46,50]. Here, γ was calculated from the mean temperature of the in-cylinder gas. The pressure and crank position data were analyzed at an equivalence ratio of $\phi = 0.26$ at approximately 1800 RPM with no load for both CSI and TPI. The calculation shows a slightly higher energy output rate for TPI and that the peak pressure occurs earlier in the expansion stroke, as shown in Fig. 7. These observations indicate that

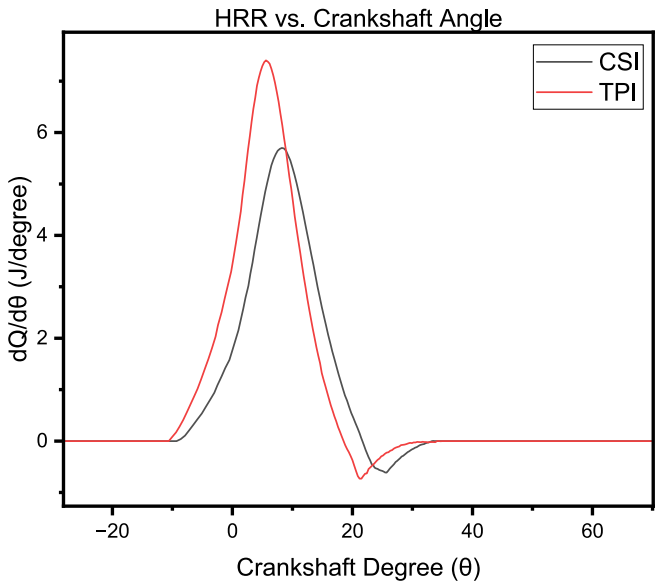



**Fig. 7.** Comparison of the heat release rate vs. crankshaft angle at $\Phi = 0.26$ at 1800 RPM with no load showing that a slightly greater heat release rate is obtainable with TPI vs. CSI.

the transient plasma ignition gives rise to a reduced ignition delay (flame development period) and promotes an increased flame speed earlier in the combustion process during the rapid burning period. Both indicate that the increased radical formation and increased flame turbulence created by the TPI can increase the engine output compared to CSI under the same engine conditions.

We attribute the observed improvement in the engine performance to the new enhancement mechanism enabled by repetitive pulses. After initiating the flame kernel triggered by the 1st pulse, it is likely that the 2nd – 5th pulses affect the shape of the kernel/flame by the strong applied electric fields since the kernel/flame behaves as a weakly ionized plasma. Specifically, such strong electric fields created by the repetitive pulses continuously apply forces to the ionized species in the initial flame kernel, which leads to the formation of ionic wind, resulting in turbulence and hydrodynamic effects. In addition, the reactive radicals (e.g., atomic H and atomic O, etc.) produced by plasma discharge further strengthen the enhancement effect discussed above due to the elevated thermodynamics and kinetics of the reaction. Such effects are reflected in the chamber pressure data and the corresponding Schlieren imaging, where significantly reduced ignition delays and faster pressure rise times (i.e., dP/dt), and increased flame surface area are demonstrated with TPI, which ultimately improves the flame stability and engine performance.

## 4. Conclusion

In conclusion, the enhanced combustion of $H_2$ in an internal combustion engine with TPI provides higher output powers and more stable operation than CSI while lowering NO emissions under ultra-lean conditions. We observed 52 % and 33 % reduction in $COV_{IMEP}$ under no load and load conditions, respectively at ultra-lean conditions (i.e., $0.2 \leq \phi \leq 0.4$), illustrating better engine stability with TPI. We observed a 50 % reduction in NO emissions with TPI for $0.5 \leq \phi \leq 0.6$ under both no load and load conditions. In addition, TPI substantially extends the stable $H_2$ combustion range. We also observe an up to 175 % increase in the maximum power output with TPI under ultra-lean conditions $0.24 \leq \phi \leq 0.3$. The transient plasma-based enhancement arises from two key mechanisms: 1.) the formation of highly reactive radical species, including atomic H and atomic O, gives rise to accelerated reaction (i.e., burn) rates, and 2.) multi-pulse high voltage discharge gives rise to ionic winds, multiscale turbulence and mixing, and increased flame surface area of the flame kernel. This is supported by Schlieren imaging, which shows an augmented flame surface area and reduced ignition delays with TPI compared to CSI. Consequently, this results in significantly reduced ignition delays and faster pressure rise times (i.e., dP/dt) with TPI compared to those observed with CSI. Ultimately, TPI supports a more robust flame kernel that gives rise to lower COV values and NO emissions via hydrodynamic effects (i.e., ionic winds) and the formation of highly reactive radical species, e.g., atomic H and atomic O. These results could have important practical implications over a wide range of engines and combustion systems and can be used as the basis for in-depth fundamental studies in canonical laboratory configurations.

## CRediT authorship contribution statement

**Boxin Zhang:** Writing – review & editing, Writing – original draft, Visualization, Validation, Methodology, Formal analysis, Data curation, Conceptualization. **Mariano Rubio:** Writing – review & editing, Writing – original draft, Visualization, Validation, Methodology, Formal analysis, Data curation, Conceptualization. **Joshua E. Tobar Lam:** Data curation. **Aimee Ortiz-Ramirez:** Data curation. **Travis Riggs:** Data curation. **Oscar Hernandez:** Data curation. **Yushan Chen:** Data curation. **Caleb Medchill:** Data curation. **Fokion Egolfopoulos:** Writing – review & editing, Project administration, Investigation, Conceptualization. **Stephen B. Cronin:** Writing – review & editing, Writing – original draft, Supervision, Project administration, Methodology, Investigation, Funding acquisition, Conceptualization.

## Declaration of competing interest

The authors declare that they have no known competing financial interests or personal relationships that could have appeared to influence the work reported in this paper.

## Data availability

Data will be made available on request.

## Acknowledgments

This research was supported by the National Science Foundation (NSF) Award No. CHE-1954834 (B.Z.), the Army Research Office (ARO) Award No. W911NF2210284 (C.M), and the USC Ershaghi Center on Energy Transition (E-CET) (M.R.). Support for this research was also provided by the Citrus College Summer Research Experience Program, through a generous donation from the Citrus College Foundation.

## Appendix A. Supplementary data

Supplementary data to this article can be found online at https://doi.org/10.1016/j.fuel.2024.133233.

## References

[1] Giuliano, G.; Dexter, S. Decarbonizing Road Freight and Alternative Fuels for Urban Logistics. In *The Routledge Handbook of Urban Logistics*, Routledge, 2023; pp 333-350. ISBN: 9781003241478.
[2] Giuliano, G.; Dessouky, M.; Dexter, S.; Fang, J. W.; Hu, S. C.; Miller, M. Heavy-duty trucks: The challenge of getting to zero. *Transportation Research Part D-Transport and Environment* 2021, *93*. DOI: 10.1016/j.trd.2021.102742.
[3] Kumar V, Gupta D, Kumar N. Hydrogen use in internal combustion engine: a review. Int J Adv Culture Technol 2015;3(2):87–99.
[4] Wallner T, Lohse-Busch H, Gurski S, Duoba M, Thiel W, Martin D, et al. Fuel economy and emissions evaluation of BMW Hydrogen 7 Mono-Fuel demonstration vehicles. Int J Hydrogen Energy 2008;33(24):7607–18.
[5] Fayaz H, Saidur R, Razali N, Anuar FS, Saleman A, Islam M. An overview of hydrogen as a vehicle fuel. Renew Sustain Energy Rev 2012;16(8):5511–28.
[6] Oikawa M, Ogasawara Y, Kondo Y, Sekine K, Takagi Y, Sato Y. Optimization of hydrogen jet configuration by single hole nozzle and high speed laser

shadowgraphy in high pressure direct injection hydrogen engines. Int J Automotive Eng 2012;3(1):1–8.
[7] Jamrozik A, Grab-Rogaliński K, Tutak W. Hydrogen effects on combustion stability, performance and emission of diesel engine. Int J Hydrogen Energy 2020;45(38):19936–47.
[8] Luo, Q.-h.; Hu, J.-B.; Sun, B.-g.; Liu, F.-s.; Wang, X.; Li, C.; Bao, L.-z. Effect of equivalence ratios on the power, combustion stability and NOx controlling strategy for the turbocharged hydrogen engine at low engine speeds. *international journal of hydrogen energy* 2019, *44* (31), 17095-17102.
[9] Sharma S, Goyal P, Tyagi R. Hydrogen-fueled internal combustion engine: a review of technical feasibility. Int J Performability Eng 2015;11(5):491.
[10] Stępień Z. A comprehensive overview of hydrogen-fueled internal combustion engines: Achievements and future challenges. Energies 2021;14(20):6504.
[11] El-Adawy M, Nemitallah MA, Abdelhafez A. Towards sustainable hydrogen and ammonia internal combustion engines: Challenges and opportunities. Fuel 2024;364:131090.
[12] Onorati A, Payri R, Vaglieco B, Agarwal A, Bae C, Bruneaux G, et al. The role of hydrogen for future internal combustion engines. SAGE Publications Sage UK: London, England 2022;23:529–40.
[13] De Boer PCT, McLean WJ, Homan HS. Performance and emissions of hydrogen fueled internal combustion engines. Int J Hydrogen Energy 1976;1(2):153–72.
[14] Ciniviz M, Köse H. Hydrogen use in internal combustion engine: a review. Int J Automotive Eng Technol 2012;1(1):1–15.
[15] White C, Steeper R, Lutz AE. The hydrogen-fueled internal combustion engine: a technical review. Int J Hydrogen Energy 2006;31(10):1292–305.
[16] Gao W, Fu Z, Li Y, Li Y, Zou J. Progress of performance, emission, and technical measures of hydrogen fuel internal-combustion engines. Energies 2022;15(19):7401.
[17] Singleton D, Pendleton S, Gundersen MA. The role of non-thermal transient plasma for enhanced flame ignition in C2H4–air. J Phys D Appl Phys 2010;44(2):022001.
[18] Cathey CD, Tang T, Shiraishi T, Urushihara T, Kuthi A, Gundersen MA. Nanosecond plasma ignition for improved performance of an internal combustion engine. IEEE Trans Plasma Sci 2007;35(6):1664–8.
[19] MacCarley, C. Study of factors influencing thermally induced backfiring in hydrogen fueled engines, and methods for backfire control. In *Proc., Intersoc. Energy Convers. Eng. Conf.;(United States)*, 1981; Univ of Denver, Colo: Vol. 2.
[20] Verhelst S, Sierens R. Hydrogen engine-specific properties. Int J Hydrogen Energy 2001;26(9):987–90.
[21] Gerbig, F.; Strobl, W.; Wimmer, A.; Eichlseder, H. Potentials of the hydrogen combustion engine with innovative hydrogen-specific combustion process. In *FISITA World Automotive Congress*, 2004; . pp 1-10.
[22] Kondo T, Iio S, Hiruma M. A study on the mechanism of backfire in external mixture formation hydrogen engines-about backfire occurred by cause of the spark plug. SAE Trans 1997:1953–60.
[23] Lucas, G.; Morris, L. The backfire problem of the hydrogen engine. In *Symposium organized by the university's internal combustion engine group, King's College, London, UK*, 1980.
[24] Do H, Im S-K, Cappelli MA, Mungal MG. Plasma assisted flame ignition of supersonic flows over a flat wall. Combust Flame 2010;157(12):2298–305.
[25] Klimov, A.; Bityurin, V.; Kuznetsov, A.; Tolkunov, B.; Vystavkin, N.; Vasiliev, M. External and internal plasma-assisted combustion. In *42nd AIAA Aerospace Sciences Meeting and Exhibit*, 2004; p 1014.
[26] Chavda, K.; Kulkarni, K. Plasma Assisted Combustion: A Review. *IOSR Journal Of Applied Physics (IOSR-JAP)* 2021, *13* (4), 26-35.
[27] Maly R. Spark ignition: its physics and effect on the internal combustion engine. Fuel economy: In road vehicles powered by spark ignition engines; 1984. p. 91–148.
[28] Shiraishi T, Urushihara T, Gundersen M. A trial of ignition innovation of gasoline engine by nanosecond pulsed low temperature plasma ignition. J Phys D Appl Phys 2009;42(13):135208.
[29] Mariani A, Foucher F. Radio frequency spark plug: An ignition system for modern internal combustion engines. Appl Energy 2014;122:151–61.
[30] Kim H, Takashima K, Katsura S, Mizuno A. Low-temperature NOx reduction processes using combined systems of pulsed corona discharge and catalysts. J Phys D Appl Phys 2001;34(4):604.
[31] Pineda DI, Wolk B, Sennott T, Chen J-Y, Dibble RW, Singleton D. The Role of Hydrodynamic Enhancement on Ignition of Lean Methane-Air Mixtures by Pulsed Nanosecond Discharges for Automotive Engine Applications. Combust Sci Technol 2017;189(11):2023–37. https://doi.org/10.1080/00102202.2017.1334647.
[32] Kuhl J, Seeger T, Zigan L, Will S, Leipertz A. On the effect of ionic wind on structure and temperature of laminar premixed flames influenced by electric fields. Combust Flame 2017;176:391–9.
[33] Ciatti SA, Wallner T, Ng H, Stockhausen WF, Boyer B. Study of combustion anomalies of H2-ICE with external mixture formation. In Internal Combust Engine Division Spring Technical Conf 2006;42061:421–7.
[34] Alderman, D.; Tremble, C.; Jiang, C.; Sanders, J. M.; Singleton, D. Initial Evaluation of Pulse Risetime on Transient Plasma Ignition for Combustion. In *2018 IEEE International Power Modulator and High Voltage Conference (IPMHVC)*, 3-7 June 2018, 2018; pp 279-282. DOI: 10.1109/IPMHVC.2018.8936811.
[35] Alderman, D.; Tremble, C.; Song, S.; Jiang, C.; Sanders, J. M.; Singleton, D. Plasma kinetics study of a repetitive 10-NS pulsed plasma ignition for combustion. In *2019 IEEE Pulsed Power & Plasma Science (PPPS)*, 23-29 June 2019, 2019; pp 1-3. DOI: 10.1109/PPPS34859.2019.9009621.
[36] Bihari, B.; Biruduganti, M. S.; Torelli, R.; Singleton, D. Performance Characterization of Alternative Ignition Systems Using Optical Tools in Natural Gas Engines. In *ASME 2018 Internal Combustion Engine Division Fall Technical Conference*, 2018; V001T01A009, Vol. Volume 1: Large Bore Engines; Fuels; Advanced Combustion. DOI: 10.1115/icef2018-9704.
[37] Biswas, S.; Ekoto, I.; Singleton, D.; Mixell, K.; Ford, P. Assessment of Spark, Corona, and Plasma Ignition Systems for Gasoline Combustion. In *ASME 2020 Internal Combustion Engine Division Fall Technical Conference*, 2020; V001T03A015, Vol. ASME 2020 Internal Combustion Engine Division Fall Technical Conference. DOI: 10.1115/icef2020-3034.
[38] Pineda, D. I.; Wolk, B.; Sennott, T.; Chen, J.-Y.; Dibble, R. W.; Singleton, D. Nanosecond Pulsed Discharge Ignition in a Lean Methane-Air Mixture. In *Laser Ignition Conference*, Argonne, Illinois, 2015/04/27, 2015; Optica Publishing Group: p T5A.2. DOI: 10.1364/LIC.2015.T5A.2.
[39] Sevik J, Wallner T, Pamminger M, Scarcelli R, Singleton D, Sanders J. Extending Lean and Exhaust Gas Recirculation-Dilute Operating Limits of a Modern Gasoline Direct-Injection Engine Using a Low-Energy Transient Plasma Ignition System. J Eng Gas Turbines Power 2016:138. 11). DOI: 10.1115/1.4033470 (acccessed 2/16/2023.
[40] Singleton DR. The physics and application of compact pulsed power to transient plasma ignition. University of Southern California; 2010.
[41] Singleton D, Pendleton SJ, Gundersen MA. The role of non-thermal transient plasma for enhanced flame ignition in C2H4–air. J Phys D Appl Phys 2011;44(2):022001. https://doi.org/10.1088/0022-3727/44/2/022001.
[42] Singleton DR, Gundersen MA. Transient Plasma Fuel-Air Ignition. IEEE Trans Plasma Sci 2011;39(11):2214–5. https://doi.org/10.1109/TPS.2011.2135380.
[43] Singleton DR, Kuthi A, Sanders JM, Gundersen MA, Simone A, Pendleton SJ. Low energy compact power modulators for transient plasma ignition. IEEE Trans Dielectr Electr Insul 2011;18(4):1084–90. https://doi.org/10.1109/TDEI.2011.5976099.
[44] Singleton DR, Sinibaldi JO, Brophy CM, Kuthi A, Gundersen MA. Compact Pulsed-Power System for Transient Plasma Ignition. IEEE Trans Plasma Sci 2009;37(12):2275–9. https://doi.org/10.1109/TPS.2009.2024672.
[45] Biswas, S.; Ekoto, I.; Singleton, D.; Mixell, K. *Nanosecond Pulsed Ignition for Automotive Applications: Performance and Emissions Characteristics of Gasoline Combustion in an Optical Engine*; SAE Technical Paper, 2021. DOI: https://doi.org/10.4271/2021-01-0475.
[46] Heywood JB. Internal combustion engine fundamentals. McGraw-Hill Education; 2018.
[47] Nagashima K, Kawa T, Tsuchiya K. Indicated mean effective pressure measuring method using optical fiber pressure sensor. SAE Trans 2003:1968–74.
[48] Zeldvich YB. The oxidation of nitrogen in combustion and explosions. J Acta Physicochimica 1946;21:577.
[49] Ju Y, Sun W. Plasma assisted combustion: Progress, challenges, and opportunities. Combust Flame 2015;162(3):529–32.
[50] Shudo T, Suzuki H. Applicability of heat transfer equations to hydrogen combustion. JSAE Rev 2002;23(3):303–8.